Inorganic Chemistry

Article

pubs.acs.org/IC

8 − *N* Rule and Chemical Bonding in Main-Group MgAgAs-Type Compounds

David Bende, Frank R. Wagner, and Yuri Grin*

Max-Planck-Institut für Chemische Physik fester Stoffe, Nöthnitzer Straße 40, 01187 Dresden, Germany

Supporting Information

ABSTRACT: The chemical bonding of main-group MgAgAs-type compounds is analyzed with quantum chemical direct-space techniques. A new bonding concept is developed that unites the former ionic bonding and polyanionic network models. Polar and nonpolar contributions to the bonding are extracted by the combined analysis of electron density and electron localizability. A direct-space representation of the 8 − *N* rule is introduced. In this approach, the anions' heteropolar bonds are treated as a superposition of covalent (nonpolar) and lone-pair closed-shell (polar) contributions. The relation between covalent (nonpolar) and lone-pair (polar) character is obtained with the ELI-D/QTAIM basin intersection technique. This ratio depends on the constituting elements. On basis of this approach, MgAgAs-type compounds are compared with Zintl phases, where covalent bonds and lone pairs are spatially separated.

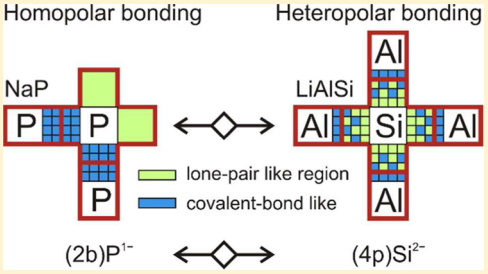

INTRODUCTION

MgAgAs-type intermetallic compounds constitute a remarkable class of materials suitable for various applications.[1]

In solar cells, the semiconducting representatives with 8 or 18 valence electrons per formula unit are "green" alternatives to the established buffer-layer material CdS in ZnO/CdS/Cu(In,Ga)Se_2 heterojunctions.[2,3] For this purpose, the lattice parameter and the band gap of MgAgAs-type compounds can be tuned according to the requirements of the light absorber.[4−6]

Thermoelectric converters are used to recover a part of the heat emission as electric energy. A materials breakthrough in this technology would greatly contribute to an environment friendly energy management. Because the structure of MgAgAs-type compounds allows chemical substitutions over a large composition range, n-type or p-type materials with the same parent compound can be designed.[7]

Furthermore, MgAgAs-type semiconductors with rare-earth and other heavy elements show interesting properties for the design of new spintronic devices: bulk magnetism (LnPtBi, Ln = Nd, Sm, Gd, Tb, Dy[8]), giant magnetoresistance (GMR in DyNiSb and TbNiSb[9]), extraordinary magnetoresistance (EMR in DyNiBi[10]), heavy-Fermion behavior (YbPtBi[11]), superconductivity (LaPtBi[12]), and topological-insulator behavior (LuPtBi[13]). The variety of different constituent combinations and the possibility to dope the MgAgAs-type compounds facilitates the discovery and study of new/combined spintronic effects, which is the basis for the design of new innovative devices.[2]

The cubic face centered MgAgAs-type crystal structure (space group $F\bar{4}3m$) is often considered to be a defect derivative of the Heusler phases with the crystal structure of the $MnCu_2Al$ type, which explains why they are also termed half-Heusler compounds. In a XYZ compound of the MgAgAs type, two of the three components, X and Y, form a rock-salt-like arrangement.[14] Z occupies half of the cubic voids of the rock-salt partial structure. Each of the so-obtained XZ and YZ arrangements separately reflects a zinc-blende pattern (Figure 1). The atoms X and Y are both coordinated tetrahedrally by Z atoms. The atom at the Z position has a heterocubic X_4Y_4 coordination (HC site). X/Y substitutional disorder leads to the antifluorite structure, like that in (LiMg)N. Therefore, an ordered substitution variant of the fluorite type is another point of view on the structural pattern of the MgAgAs type.

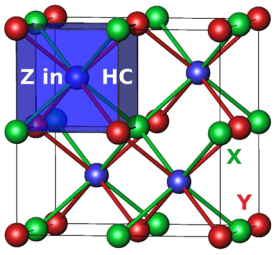

Figure 1. Crystal structure of MgAgAs-type compounds. The green and red sticks indicate the two interpenetrating zinc-blende patterns. The heterocubic coordination of the central blue atom is highlighted.

Depending on the component that occupies the heterocubic site there are three possible, chemically different, atomic arrangements. In the following, the specific atomic arrangement is described by a superscript indicating the element at the heterocubic site, e.g., $MgAgAs^{HC}$.

Received: January 20, 2015
Published: April 3, 2015

DOI: 10.1021/acs.inorgchem.5b00135
Inorg. Chem. 2015, 54, 3970−3978

MgAgAs-type compounds can be composed of many elements. Combinations of two early main-group elements A′A or two transition metals T′T with a late main-group element E, A′AE, and T′TE, respectively, are possible. ATE and rare-earth (R) phases RTE are also known. Each of these groups, except the ATE compounds, occurs only with one atomic arrangement: $A'AE^{HC}$, $T'T^{HC}E$, $RT^{HC}E$, and ATE^{HC} or $AT^{HC}E$.

The first description of chemical bonding in MgAgAs-type semiconductors on the basis of the ionic bonding model was presented in the pioneer papers by Nowotny[14] and Juza.[15] The constant composition and the absence of defects of the $A'AE^{HC}$ and ATE^{HC} compounds were taken as an indication of the ionic character. Assuming the formal charge assignment, e.g., $Mg^{2+}Ag^{+}As^{3-}$, the anion at the heterocubic site is surrounded by eight cations, which is favorable for ionic interactions. On the contrary, in $AT^{HC}E$ and $T'T^{HC}E$ compounds, ionic interactions do not play the decisive role because the arrangement of the charges is unfavorable.[16]

The model of the polyanionic network describes chemical bonding in MgAgAs-type semiconductors as a combination of ionic and covalent interactions.[17] The least electronegative component X transfers its n valence electrons to the polyanion $[YZ]^{n-}$. Thereby, cation and polyanion realize a closed-shell electronic configuration. The view of the polyanionic network is considered to be consistent with the phonon spectra,[18] the analysis of the density of states (DOS) and crystal orbital overlap populations (COHP),[19] the distribution of valence charge density, and the analysis of the valence part of the electron localization function (valence ELF).[19] The model is formally applicable to all 8- and 18-electron MgAgAs-type compounds. However, the T′TE and RTE semiconductors show additional bonding features, i.e., T′/R−T covalent interactions[19,20] and three-center bonds.[21]

In an attempt to develop a more general bonding concept, the present analysis initially covers main-group MgAgAs-type semiconductors. They are all treated equally and analyzed by quantum chemical methods in real space. The real-space techniques have already proven to be a potent model framework to reveal different types of bonding interactions in MgAgAs-type semiconductors.[16] This allows a consistent and comparative study of the chemical bonding in these substances and opens a way to reformulate the $8 - N$ electron rule for compounds that do not belong to the Zintl phases.

METHODS

The lattice parameters of the MgAgAs-type compounds were optimized within density functional theory using the PBE exchange-correlation functional[22] and the augmented plane-wave method including local orbitals (APW + lo), as implemented in the Elk code.[23] The program DGrid[24] was used to obtain quantum chemical real-space bonding indicators (see Supporting Information for computational details). Within the quantum theory of atoms in molecules (QTAIM), solely the electron density is used to define atomic regions (QTAIM atoms) in position space. The QTAIM atomic regions (basins of the electron density maxima) Ω_X and their effective atomic charges $Q^{eff}(\Omega_X)$ are physically well-defined.[25] We will no longer distinguish between QTAIM atomic regions Ω_X and atomic species X: $\Omega_X \equiv X$. Electron sharing between the space-filling and nonoverlapping QTAIM atoms is quantified via two-center delocalization indices (DI) $\delta(X,Y)$, which are interpreted as a measure of covalent bond order. For example, DI values of 1.01, 1.98, and 2.89 have been found for the C−C bonds in C_2H_6, C_2H_4, and C_2H_2, respectively.[26] The calculation of DIs for crystalline solids has been realized recently.[27] The three-center delocalization indices $\delta(X,Y,Z)$ and the related bond G-value are used to characterize the delocalization of a bond X−Y.[28] $G(X,Y) = 1$ classifies an X−Y bond as being three-center-like delocalized.

$$G(X,Y) = \frac{\sum_{Z\neq X,Y} \delta(X,Y,Z)}{\delta(X,X,Y) + \delta(X,Y,Y)} \quad (1)$$

The topological analysis of the electron localizability indicator (ELI-D, Y_D^{σ})[29] complements the QTAIM analysis. ELI was proven to be a potent quantum chemical technique for bonding analysis in crystalline compounds, particularly also in the intermetallic phases.[30,31] For systems described by a monodeterminantal closed-shell time-independent wave function, ELI-D has an identical topology as the ELF.[32] As an important property ELI-D is known to display atomic shell structure in position space, i.e., isolated atoms exhibit an onion-like topology with a spherical ELI-D maximum for each atomic shell and a spherical minimum in between. The number of such shell regions corresponds to the main quantum number and the periodic table of the elements. The electronic shell populations are very close but not identical to the integral numbers given by the Aufbau principle.[33,34] For molecules and solids, the inner atomic shells remain virtually unchanged, but the local maxima (attractors) of Y_D^{σ} in the valence region are considered to be topological fingerprints of atomic interactions in the direct-space quantum chemical techniques for bonding analysis.[30,31] The points of space around an attractor connected to it by lines of steepest ascent (gradient paths) form the basin (catchment region) of this attractor. ELI-D attractors and associated basins B_i in the valence region between the atoms indicate lone-pair regions or covalent bonds.[35] The ELI-D/QTAIM intersection technique (analogous to ref 36) is applied to assess the bond polarity of ELI-D valence regions. In this way, a segmentation of ELI-D valence basins with the QTAIM basins is performed ("cut the bond by the atoms"). The bond fraction p quantifies to what extent the neighboring QTAIM atoms contribute electrons to an ELI-D basin. For an atom X intersecting the ELI-D basin B_i, the bond fraction is calculated as

$$p(B_i^X) = \frac{\bar{N}(B_i^X)}{\bar{N}(B_i)} \quad (2)$$

where $\bar{N}(B_i)$ is the number of electrons in an ELI-D basin B_i, obtained by integration of the electron density, $\bar{N}(B_i^X)$ is the number of electrons in the intersected region B_i^X of the ELI-D valence basin B_i with the QTAIM basin Ω_X. The value of p ranges between 0 and 1. A value of $p = 1$ indicates a nonintersected, monatomic ELI-D valence basin, which is interpreted as an electron lone pair. For a diatomic ELI-D valence basin intersected by two QTAIM basins, $p = 0.5$ represents the case of a nonpolar covalent bond, as both QTAIM basins contribute the same amount of electrons to that region. All intermediate values stand for polar covalent bonding.

In order to classify the overall bonding pattern in terms of the ELI-D/QTAIM intersection, the access electron number $\bar{N}_{acc}^{ELI}(C^X)$ and the valence electron number $\bar{N}_{val}^{ELI}(X)$ are introduced

$$\bar{N}_{acc}^{ELI}(C^X) = \sum_{i=1}^{s_X} \bar{N}(B_i) \quad (3)$$

where s_X is the number of ELI-D bonding basins B_i sharing surface with the ELI-D core basin C^X. These basins constitute the access set of atom X. Accordingly, the access electron number indicates the number of valence electrons that C^X is surrounded by/has access to. The valence electron number is calculated as the difference between the overall QTAIM basin population $\bar{N}(\Omega_X)$ and the ELI-D core basin population $\bar{N}(C^X)$.

$$\bar{N}_{val}^{ELI}(X) = \bar{N}(\Omega_X) - \bar{N}(C^X) \approx \sum_{i=1}^{s_X} \bar{N}(B_i^X) \quad (4)$$

The approximate equality appears because atom X may contribute electrons to an ELI-D valence basin that does not have a common surface with its core C^X. The amount of such contributions in the

DOI: 10.1021/acs.inorgchem.5b00135
Inorg. Chem. 2015, 54, 3970−3978

Table 1. Real-Space Bonding Analysis of Main-Group MgAgAs-Type Semiconductors[a]

A′AE	LiMgN	LiMgP	LiMgAs	LiMgSb	LiMgBi	LiAlSi	LiAlGe	LiInGe	LiInSn	AlBeB[b]
a_{exp}	4.995[39]	6.003[40]	6.181[41]	6.60[42]	6.73[42]	5.922[43]	5.977[43]	6.304[44]	6.676[44]	4.93[45]
a_{opt}	5.003	6.014	6.212	6.672	6.865	5.937	6.020	6.404	6.820	4.962
QTAIM Analysis										
$Q^{eff}(A')$	+0.81	+0.83	+0.83	+0.84	+0.84	+0.82	+0.83	+0.84	+0.84	+2.08
$Q^{eff}(A)$	+1.57	+1.49	+1.46	+1.39	+1.31	+1.40	+1.34	+0.18	0.00	+1.42
$Q^{eff}(E)$	−2.38	−2.32	−2.29	−2.23	−2.15	−2.22	−2.16	−1.02	−0.84	−3.50
$\delta(A',A)$[c]	0.040	0.004	0.003	0.003	0.004	0.010	0.010	0.015	0.014	0.009
$\delta(A',E)$	0.102	0.084	0.081	0.077	0.074	0.072	0.070	0.048	0.046	0.352
$\delta(A,E)$	0.222	0.232	0.240	0.259	0.278	0.538	0.536	0.688	0.681	0.208
ς_{nn}	1.33	1.27	1.28	1.34	1.41	2.44	2.42	2.95	2.91	2.24
$G(A,E)$	0.22	0.26	0.28	0.29	0.33	0.36	0.35	0.32	0.35	0.56
ELI-D Basin $_{3A',A,E}B$: Four Basins Per Formula Unit, Pentasynaptic (3A′,1A,1E)										
$\bar{N}(_{3A',A,E}B)$	1.94	1.94	1.92	1.64	1.54	1.95	2.02	1.85	1.52	0.99
$p(B^{A'})$/%	1.8	1.6	1.4	0.7	0.3	1.7	1.5	1.2	0.6	3.5
$p(B^{A})$/%	4.5	5.5	6.0	8.0	9.8	19.5	19.6	34.3	43.0	12.5
$p(B^{E})$/%	93.7	92.9	92.6	91.3	89.9	78.8	78.9	64.5	56.4	84.1
ELI-D Basin $_{A',E}B$: Four Basins Per Formula Unit, Disynaptic (1A′,1E)										
$\bar{N}(_{A',E}B)$	–	–	0.10	0.39	0.52	–	–	0.14	0.41	0.95
$p(B^{A'})$/%	–	–	4.5	5.4	4.9	–	–	5.4	5.2	18.2
$p(B^{E})$/%	–	–	95.5	94.6	95.1	–	–	94.6	94.8	81.8
$\bar{N}^{ELI}_{acc}(C^{E})$	7.76	7.76	8.08	8.12	8.24	7.80	8.08	7.96	7.72	7.76
$P_E(A'_{tot})$/%	1.8	1.6	1.6	1.6	1.5	1.7	1.5	1.5	1.5	10.6
$P_E(A_{tot})$/%	4.5	5.5	5.7	6.5	7.3	19.5	19.6	31.9	33.9	6.4
$P_E(E)$/%	93.7	92.9	92.7	91.9	91.2	78.8	78.9	66.6	64.6	83.0
$CI3_E$/%	18	20	20	23	24	51	51	68	70	44
8 − N Rule in Direct Space										
$\bar{N}^{ELI}_{val}(E)$	7.26	7.24	7.53	7.47	7.52	6.14	6.43	5.28	4.99	6.42
$lpc(_{3A',A,E}B^{E})$/%	87	86	85	83	80	58	58	29	13	68
$lpc(_{A',E}B^{E})$/%	–	–	91	89	90	–	–	89	90	64
$N_{cb}(E)$	0.50	0.52	0.55	0.65	0.72	1.66	1.65	2.68	2.73	1.34
$N_{lp}(E)$	3.39	3.33	3.45	3.40	3.39	2.25	2.34	1.32	1.13	2.56

[a] a_{exp} and a_{opt}, experimental and optimized lattice parameters; Q^{eff}, QTAIM effective charge; δ, delocalization index; ς_{nn}, nearest neighbor sharing; $G(A,E)$, delocalized character of bond A−E; $\bar{N}$, average number of electrons; p, bond fraction; $CI3_E$, connection index for the set s_E; $\bar{N}^{ELI}_{acc}(C^E)$, number of ELI-D access electrons for species E; $\bar{N}^{ELI}_{val}(E)$, number of ELI-D valence electrons for species E; lpc, lone-pair character in percent; $P_E(E)$, genuine charge claim of E; $P_E(A'_{tot})$ and $P_E(A_{tot})$, summarized residual charge claims of A′ and A for the set s_E; N_{lp}, number of lone pairs (according to the presented formalism); N_{cb}, number of covalent bonds (according to the presented formalism). [b] The order of components is chosen such that the charge fraction block can be read correctly (disynaptic ELI-D basin is between Al and B). [c] This delocalization index does not contribute to ς_{nn} because the components form the rock-salt partial structure.

analyzed compounds is negligible. For an access electron set s_X of valence basins, the genuine charge claim $P_X(X)$ represents the average bond fraction of atom X within its access set

$$P_X(X) = \frac{\sum_{i=1}^{s_X} p(B_i^X)\cdot\bar{N}(B_i)}{\sum_{i=1}^{s_X}\bar{N}(B_i)} = \frac{\sum_{i=1}^{s_X}\bar{N}(B_i^X)}{\bar{N}^{ELI}_{acc}(C^X)} \approx \frac{\bar{N}^{ELI}_{val}(X)}{\bar{N}^{ELI}_{acc}(C^X)} \quad (5)$$

The subscript in $P_X(X)$ refers to the set of ELI-D valence basins s_X and the atom in parentheses indicates for which atom the bond fraction B_i^X is calculated. The residual charge claims $P_X(Y)$, $P_X(Z)$, etc. of the remaining contributors Y, Z, etc. for the chosen access set of X can be calculated according to

$$P_X(Y) = \frac{\sum_{i=1}^{s_X} p(B_i^Y)\cdot\bar{N}(B_i)}{\sum_{i=1}^{s_X}\bar{N}(B_i)} = \frac{\sum_{i=1}^{s_X}\bar{N}(B_i^Y)}{\bar{N}^{ELI}_{acc}(C^X)} \quad (6)$$

The sum of genuine charge claim and residual charge claims for the access set is unity. The residual charge claims of equivalent atoms are summarized in Table 1 for A′ ($P_E(A'_{tot})$) and A ($P_E(A_{tot})$; see the Supporting Information for a representative example.

For further characterization of the bonding patterns within the ELI-D/QTAIM intersection and QTAIM/DI representation, two quantities are proposed: the connection index CIn and the nearest neighbor sharing ς_{nn}, respectively. The connection index condenses the variety of different bond fractions into one number

$$CIn_X = \frac{2n}{n-1}\sum_{Y<Z}[P_X(Y)\cdot P_X(Z)] \quad (7)$$

where n is the number of components with a nonzero charge claim (see the Supporting Information for an representative example). The connection index adds pairwise products of charge claims, each of which being an average of individual bond fractions. Each such product represents a measure of the equality of the two bond fractions and can be thought to mimic in a coarse-grained fashion the basic construction principle of the Fulton sharing index,[37] which displays the same bond values at a single determinant level of theory[38] as the delocalization index. The most simple case occurs when the access electron set of one component contains all different ELI-D valence basins. Otherwise, additional connection indices CIn_Y, CIn_Z, etc. have to be calculated to describe the bonding of a compound completely. The sum in eq 7 runs over all combinations of component pairs. The prefactor of the sum is the normalization constant to scale the connection index between 0 and 1. For n = 2, like that in diatomic molecules and solids with one kind of bond only such as diamond, zinc-blende, or rock-salt-type phases, the connection index simply reflects the bond polarity (see Table S2), and eq 7 reduces to $CI2_X = 4\cdot P_X(X)\cdot[1 - P_X(X)]$ due to $P_X(Y) = 1 - P_X(X)$. For increasingly polar bonding along diamond,

DOI: 10.1021/acs.inorgchem.5b00135
Inorg. Chem. 2015, 54, 3970−3978

GaAs, and BeS, the connection index decreases from $CI2_C$ = 4·0.5·0.5 = 1 (nonpolar bonding) to $CI2_S$ = 4·0.95·0.05 = 0.19 (highly polar bonding). For MgAgAs-type semiconductors A′AE, n = 3. To obtain the connection indices for the analyzed compounds, it is sufficient to examine the charge claims of the access electron set of the late main-group element E because it contains the complete variety of different ELI-D basins. A value of $CI3_E$ = 1 corresponds to the situation of an equal electron contribution of all components to the bonding region, i.e., $P_E(E) = P_E(A) = P_E(A') = {}^1/_3$. Again, this represents the case of nonpolar covalent interactions within the ELI-D/QTAIM intersection. The connection index of a compound becomes zero in a completely ionic bonding situation when all of the valence electrons are contained in the QTAIM basins of one component. The connection index for the polyanionic network model is 0.75.

The nearest neighbor sharing ς_{nn} sums all delocalization indices that occur between nearest neighbors of a compound, i.e., within the two zinc-blende partial structures. For A′AE compounds (cf. ref 16)

$$\varsigma_{nn}(A'AE^{HC}) = 4\delta(A',E^{HC}) + 4\delta(A,E^{HC}) \quad (8)$$

which summarizes the energetically most significant covalent interactions.[16]

RESULTS AND DISCUSSION

Ten A′AE compounds, LiMgN, LiMgP, LiMgAs, LiMgSb, LiMgBi, LiAlSi, LiAlGe, LiInGe, LiInSn, and BeAlB, are analyzed. For all of these MgAgAs-type semiconductors, the optimized lattice parameters agree well with the experimental data (Table 1), which indicates the physical relevance of the calculated electronic structures.

The QTAIM effective charges indicate that the two early main-group elements play the role of cations and that the late main-group element is the only anion (Figure 2 and Table 1; cf.

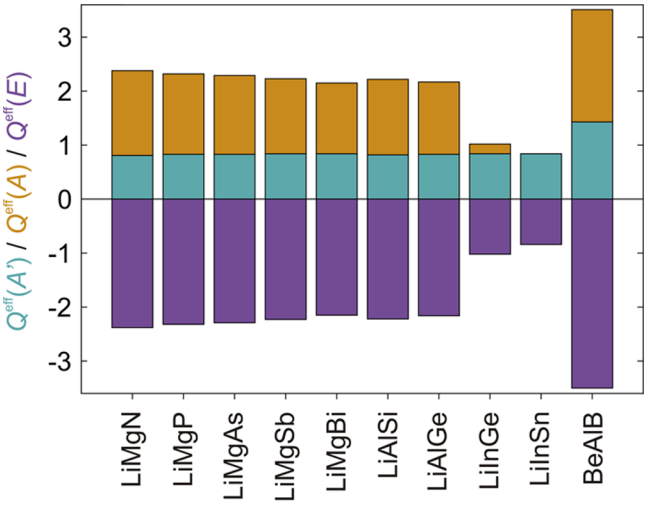

Figure 2. QTAIM effective charges (Q^{eff}) of the MgAgAs-type A′AE compounds.

ref 16.). In general, the charge distribution pattern of the A′AE compounds is consistent with the ionic bonding model. In particular, the pnictides LiMgE are well-described by this concept. Less ionic compounds, like LiInE, should show significant covalent bonding. BeAlB shows by far the largest charge separation, $Q^{eff}(B) = -3.5$.

The bonding patterns in the A′AE compounds are presented in the form of the spatial distributions of the ELI-D. In the A′AE compounds, ELI-D adopts two different topologies (Figure 3).

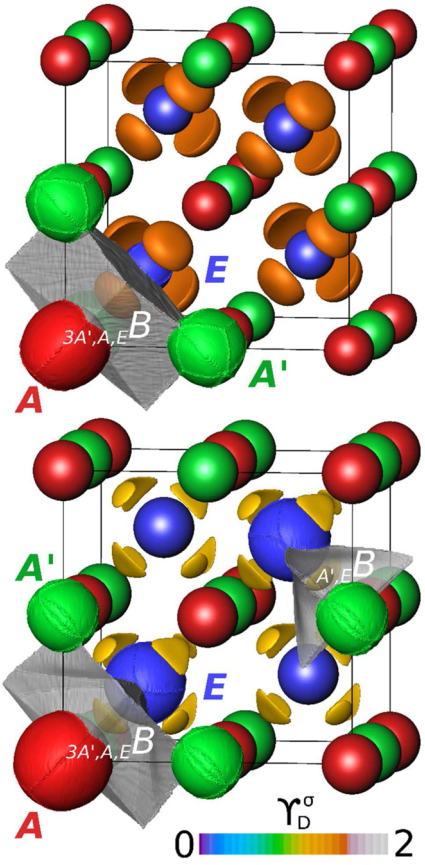

Figure 3. Two ELI-D topologies in A′AE compounds with one (top) and two (bottom) types of attractors. The isosurfaces visualize the location of ELI-D maxima: $LiMgP^{HC}$, ELI-D isovalue = 1.500 (top); $LiInSn^{HC}$, isovalue = 1.135 (bottom). The pentasynaptic basin ${}_{3A',A,E}B$ is shown in the lower left corner; the disynaptic basin ${}_{A',E}B$ appears on the right side. Each atomic core basin that touches one of the bonding basins is shown.

Around each atom at the heterocubic site in compounds LiAlSi, LiAlGe, LiMgN, and LiMgP, there are four equal ELI-D bonding attractors on the interconnection line to either aluminum or magnesium (Figure 3, top). The corresponding ELI-D basins ${}_{3A',A,E}B$ are populated by two electrons ($\bar{N}({}_{3A',A,E}B)$, Table 1). The subscript describes the synaptic-ity[46−48] of the ELI-D basin B, i.e., the number of atomic core basins with which the given valence basin has a common surface. Each basin ${}_{3A',A,E}B$ touches five core basins of neighboring atoms (pentasynaptic basin). Apart from the two cores of the two most electronegative elements A and E, additional three cores of the most electropositive component, 3A′, forming a regular triangle share a surface with the bonding basin (Figure 3).

The remaining A′AE compounds, LiInGe, LiInSn, LiMgAs, LiMgSb, LiMgBi, and BeAlB, show an ELI-D topology where each anion at the heterocubic site is surrounded by eight (4 + 4) ELI-D maxima (Figure 3, bottom). In all cases A′AE, the four new maxima occur on the direct connection line of the most electronegative component E on the heterocubic site and the most electropositive component A′ (in BeAlB, A′ = Al). These new basins ${}_{A',E}B$ are disynaptic. The total electronic population of a pair of one pentasynaptic and one disynaptic basin is two. In the majority of cases, the electron populations

DOI: 10.1021/acs.inorgchem.5b00135
Inorg. Chem. 2015, 54, 3970−3978

of basins $_{3A',A,E}B$ and $_{A',E}B$ are very different, and only in BeAlB are they similar (Table 1).

Within the sequences LiMgN, LiMgP, LiMgAs, LiMgSb, LiMgBi, LiAlSi, LiAlGe, LiInGe, and LiInSn the ELI-D topology changes from that with one type of attractors to the other one with two types of attractors between the second and the third compound in each sequence. Appearance of the second kind of attractor (basin $_{A',E}B$) is the result of a bifurcation process[25] that occurs due to the electronegativity and size difference between the components. Analysis of the ELI-D Laplacian[31] (see Supporting Information) and the discussion below characterize the topological change as part of a gradual development. The presence of different ELI-D distribution patterns within one crystallographic structure type seems to originate in the chemical nature of the components and, if a gradual topological development between different patterns is possible, does not mean different patterns of chemical bonding. One of the reasons for a gradual development is the difference in electronegativity of the components, which influences the bond polarity.

In order to assess the bond polarity, the ELI-D/QTAIM basin intersections were calculated. The pentasynaptic ELI-D basins all have in common that the three bond fractions of the most electropositive component (aluminum in BeAlB) are very small. Thus, we classify them hereafter as effectively diatomic at most. The bond fractions of the two remaining components vary within a wide range. In LiMgPn (Pn = pnictide), the pentasynaptic basins are mainly monatomic in character, as the bond fraction of the pnictide is always larger than 89%. Such effectively monatomic ELI-D basins are conceptually equivalent to lone pairs. In the following, they will be termed lone-pair-like.

From BeAlB to LiAlSi and from LiAlGe to LiInGe and LiInSn, the bond fraction of the most electronegative component decreases. In LiInSn, the pentasynaptic basin corresponds to a slightly polar bond with a bond fraction of tin of 56% and a bond fraction of indium of 43%. The disynaptic basins almost always correspond to lone-pair regions of the anion ($p(B^E)$ > 94%). Only in BeAlB do the bond fractions indicate certain two-center character of the disynaptic basin, as the bond fraction of aluminum is 18%. Further quantitative characterization of the gradual topological development of the bonding pattern was obtained applying the charge claims and connection and delocalization indices (cf. Methods).

The charge claims (eqs 5 and 6) obtained for the A′AE compounds are related to the two extreme (reference) bonding model cases, the ideal ionic bonding, and the ideal polyanionic network (Table 1 and Figure 4). The set s_E of the late main-group element E contains all various ELI-D valence basins and completely describes the bonding. s_E is 4 or 8 for the two ELI-D topologies in Figure 3. In an ideal polyanionic network, the most electropositive component A′ contributes all of its valence electrons to the polyanion ($P_E(A')$ = 0). The components comprising the polyanion [AE] form a nonpolar bond in an ideal case, which corresponds to the charge claims $P_E(E)$ = $P_E(A_{tot})$ = 0.5. In an ideal ionic compound, the two early main-group elements A′ and A transfer all of their valence electrons to the most electronegative component E, leading to a charge claim of 100%, i.e., $P_E(E)$ = 1 and $P_E(A'_{tot})$ = $P_E(A_{tot})$ = 0. The intermediate cases with $P_E(E) > 0.5 > P_E(A_{tot})$ and $P_E(A')$ = 0 are considered to be a polyanionic network with polar bonding within the polyanion.

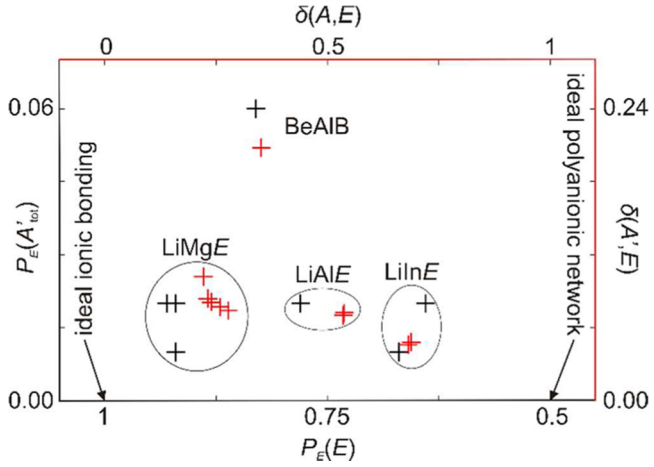

Figure 4. Real-space bonding indicators for A′AE compounds quantify their relation to the extreme bonding models. Red crosses refer to the delocalization indices representation (top *x*-axis and right *y*-axis, δ(A E) and δ(A′,E), respectively); black crosses refer to the charge claim representation (bottom *x*-axis and left *y*-axis, $P_E(A_{tot})$ and $P_E(E)$, respectively).

The delocalization indices were calculated to complement the ELI-D/QTAIM topological analysis. First, the bond orders (delocalization indices) were derived for the extreme bonding models. In the view of the polyanionic network, no electron sharing between the most electropositive component A′ and the remaining two components is expected: δ(A′,E) = 0 and δ(A′,A) = 0. Ideally, a nonpolar single bond occurs between the two more electronegative components that form the polyanion corresponding to a delocalization index δ(A,E) = 1. Within the ionic bonding model, no electron sharing occurs according to δ(A,E) = 0 and δ(A′,E) = 0.

The A′AE compounds show a bonding pattern in-between the two extreme models for both ELI-D/QTAIM and QTAIM/DI direct-space bonding representations. In all cases, except BeAlB, the most electropositive component does not participate in covalent interactions, i.e., $P_E(A'_{tot})$, δ(A′,E), and δ(A′,A) are small (Figure 4 and Table 1). The bonding picture in LiInSn and LiInGe (LiInE) gets close to the reference model of the polyanionic network. The large delocalization index between indium and the tetrel indicates sizable nonpolar interactions. Accordingly, the charge claims of the latter two elements are closest to the ideal value of 0.5. The bonding pattern of LiAlSi and LiAlGe (LiAlE) is similar to the one of LiInGe and LiInSn but with a more polar bond between the aluminum and the tetrels (larger $P_E(E)$/smaller δ(Al,E)). The pnictides LiMgE show the largest proximity to the ionic bonding model. With increasing electronegativity of the pnictide, the residual charge claim of Mg (7% ≥ $P_E(Mg)$ ≥ 4%)/the electron sharing between the two most electronegative components, Mg and E, decreases (0.28 ≥ δ(Mg,E) ≥ 0.22). In the pnictides, the value of δ(Li,E) is very low (0.10 ≥ δ(Li,E) ≥ 0.07). BeAlB does not fit well into both reference bonding models due to quite pronounced covalent Be−B interaction (Figure 4 and Table 1). The Al−B bond has a polar character in-between the pnictide and the Al−tetrel group. Thus, with respect to the bonding pattern, BeAlB is a unique representative among the A′AE compounds.

The connection indices and the nearest neighbor sharing of the MgAgAs-type semiconductors reflect the trend found in the analysis of the bond fractions and delocalization indices. Ideally,

DOI: 10.1021/acs.inorgchem.5b00135
Inorg. Chem. 2015, 54, 3970−3978

$CI3_E$ = 0 and ς_{nn} = 0 for the ionic bonding model and $CI3_E$ = 0.75 and ς_{nn} = 4 for the polyanionic network model (Figure 5).

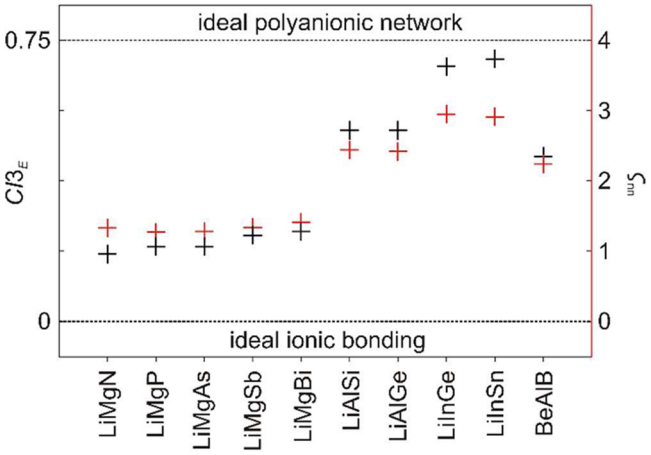

Figure 5. Connection index $CI3_E$ (black crosses) and nearest neighbor sharing ς_{nn} (red crosses) for A′AE compounds in the context of the reference bonding models.

The A′AE compounds show connection indices between 0.18 and 0.70 as well as a nearest neighbor sharing between 1.27 and 2.95. The degrees to which a compound is associated with the reference bonding models are similar for both direct-space indicators, ς_{nn} and $CI3_E$ (Figure 5). The differences between the data points of both views become even more uniform when calculated values of rock salt and silicon are used for the scaling between covalent and ionic bonding instead of the conceptual ones; see the Supporting Information.

Three-center interaction is not present in both reference bonding models. The calculated values of the three-center characters G for the two-center bonds justify this assumption (Table 1). They range between 0.21 and 0.36, which is comparable with classical two-center bonds in the diamond structure of carbon (G(C,C′) = 0.21) or germanium G(Ge,Ge′) = 0.30). Only BeAlB shows a larger G(Al,B) of 0.56, indicating a significant three-center character of the Al−B interaction. This result is consistent with the significant covalent Al−B and Be−B interactions and corroborates the particularity of the bonding scenario in BeAlB.

On the basis of the ELI-D/QTAIM basin intersection technique, the decomposition of the ELI-D bonding basin populations into polar and nonpolar contributions is developed. In the case of closed-shell interactions, the bonding basin is monatomic and represents a lone pair, and for homopolar and heteropolar bonding, the ELI-D valence basin is di- or multiatomic. In a homopolar bond, the atoms contribute an equal number of electrons to the bonding basin. These electron numbers are considered to be the nonpolar contribution (Figure 6, left). Closed-shell interaction represents the opposite case from that of homopolar bonding. The valence region between the two ELI-D core basins completely belongs to one QTAIM atom displaying ultimate polar character of the interactions (Figure 6, right). This situation is characteristic for ionic and van der Waals interactions.

In the case of a heteropolar bond, the atoms involved possess different electron numbers within the bonding basin. The nonpolar part of each atom has the same value. It is determined by the minority contributing species, e.g., A′ with $p(B^{A'}) \leq 0.5$. The remaining electrons constitute the polar part of the

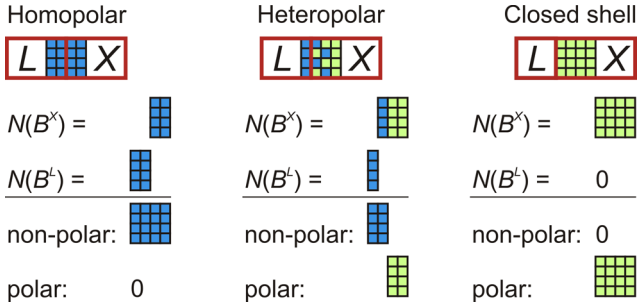

Figure 6. ELI-D representation for the homopolar, heteropolar, and closed-shell bonding situations: the thick red lines represent the atomic boundaries of QTAIM atoms X and L; the ELI-D core basins appear as white squares; the blue-green colored part represents the bonding basin with the total electronic population always symbolized by 16 minisquares. The blue minisquares symbolize the nonpolar part; the green minisquares symbolize the polar part of the bond basin population.

heteropolar bond (Figure 6, middle). This approach is related to an early view concerning the nature of partially ionic bonds in zinc-blende semiconductors, where the hypoelectronic species (the atom with less than four valence electrons) determines the covalence of the bond.[49] The decomposition of the bonding basin part B^X (green and blue minisquares) is made only to illustrate the electron populations. There is no real spatial separation between the electrons counted to the nonpolar and polar contributions.

The nonpolar contribution may be termed as the covalent part of the heteropolar bond; the polar contribution may be termed the hidden lone-pair part of the heteropolar bond. The nonpolar (covalent) character (cc) and the polar (hidden lone-pair) character (lpc) of a diatomic heteropolar ELI-D bonding basin can be calculated according to

$$\begin{aligned} \mathrm{cc}(B) &= -2p(B^X) + 2 \\ \mathrm{lpc}(B) &= 2p(B^X) - 1 \\ \mathrm{lpc}(B) + \mathrm{cc}(B) &= 1 \end{aligned} \tag{9}$$

where X is the majority contributing species with $p(B^X) \geq 0.5$. Equations 9 allow the quantification of the bond polarity: the case of cc = 1 (lpc = 0) represents the nonpolar bond, and the case of lpc = 1 (cc = 0) reflects the fully polar (closed-shell) interaction. The bonding characters cc(B) and lpc(B) are used to calculate the number of two-electron covalent bonds N_{cb}(E) and two-electron lone pairs N_{lp}(E) for the component E of the A′AE compounds with the access electron set s_E (Table 1).

$$N_{cb}(\mathrm{E}) = \frac{1}{2}\sum_{i}^{s_E} \mathrm{cc}(B_i)\cdot\bar{N}(B_i) \tag{10}$$

$$N_{lp}(\mathrm{E}) = \frac{1}{2}\sum_{i}^{s_E} \mathrm{lpc}(B_i)\cdot\bar{N}(B_i) \tag{11}$$

Equivalently, N_{cb}(E) and N_{lp}(E) can be obtained from the charge claims (eqs 12 and 13 and Figure 7).

$$\begin{aligned} N_{cb}(\mathrm{E}) &= [1 - P_E(\mathrm{E})]\cdot\bar{N}_{acc}^{ELI}(C^E) \\ &\approx \bar{N}_{acc}^{ELI}(C^E) - \bar{N}_{val}^{ELI}(\mathrm{E}) \end{aligned} \tag{12}$$

DOI: 10.1021/acs.inorgchem.5b00135
Inorg. Chem. 2015, 54, 3970−3978

$$N_{lp}(E) = \left[P_E(E) - \frac{1}{2}\right]\cdot \bar{N}_{acc}^{ELI}(C^E)$$
$$\approx \bar{N}_{val}^{ELI}(E) - \frac{1}{2}\bar{N}_{acc}^{ELI}(C^E) \quad (13)$$

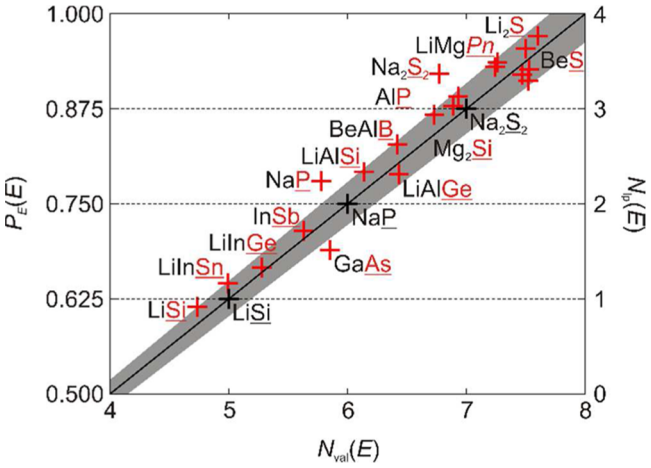

Figure 7. 8 − N rule from the ELI-D/QTAIM perspective for MgAgAs-type and related compounds. The black line represents eq 5 with $\bar{N}_{acc}^{ELI}(C^E) = 8$. Black crosses and formulas mark conceptual fixpoints of compounds that formally fulfill the 8 − N rule. The underlined element represents the hyperelectronic species E.[49] The red crosses mark the charge claims (or numbers of lone pairs) and valence electron numbers obtained from the direct space analysis.

Combination of eq 11 and 13 yields the relation

$$2[N_{cb}(E) + N_{lp}(E)] = \bar{N}_{acc}^{ELI}(C^E) \quad (14)$$

The calculated $N_{cb}(E)$ and $N_{lp}(E)$ are not necessary integers. $N_{cb}(E)$ ranges between 0.50 (LiMgN) and 2.73 (LiInSn) for the MgAgAs-type compounds (Table 1). The second part of eq 12 represents the 8 − N rule within the ELI-D/QTAIM framework for $\bar{N}_{acc}^{ELI}(C^E) = 8$ and $\bar{N}_{val}^{ELI}(E) \rightarrow N$. Accordingly, $\bar{N}_{acc}^{ELI}(C^E) = 8$ resembles the octet rule and means that an electron octet in the ELI-D/QTAIM representation is complete when an atomic core basin C^E is surrounded by basins with eight valence electrons in total to achieve a noble gas configuration.

Originally, the octet rule is formulated starting from the orbital picture of the s- and p-elements having the coordination number four. In this consideration, the lone pair plays the role of a ligand. So, silicon atoms $(3b)Si^{1-}$ in LiSi form three homonuclear bonds according to the 8 − N rule and obtain pseudotetrahedral coordination. In the ELI-D representation, the octet rule can be formulated more generally also for other coordination numbers, i.e., for $CN = 8$ of the E component in MgAgAs-type compounds.

The black line in Figure 7 represents the 8 − N rule in an idealized ($\bar{N}_{acc}^{ELI}(C^E) = 8$) ELI-D/QTAIM framework. The Zintl-phases LiSi, NaP, and Na_2S_2 with 1, 2, and 3 lone pairs and 5, 6, and 7 valence electrons per anion were used as conceptual compounds representing precise solutions of eq 5 with $\bar{N}_{acc}^{ELI}(C^E) = 8$ (Figure 7, black crosses).

The calculated values for A′AE compounds deviate slightly from the ideal line within the limits of $\bar{N}_{acc}^{ELI}(C^E) = 8 \pm 0.3$ (Table 1 and Figure 7, gray region). This implies a bonding pattern in agreement with the 8 − N rule for the MgAgAs-type compounds. Accordingly, their valence regions B^E contain between 1 and 3.5 hidden lone pairs (Figure 7). The small deviation ±0.3 originates from the ELI-D shell populations, which does not sharply match the integer values from the Aufbau principle.[33,34]

The zinc-blende-type phases InSb, GaAs, AlP, BN, and BeS, the antifluorite-type phases Mg_2Si and Li_2S, as well as the Zintl phases LiSi, NaP, and Na_2S_2 were included in the diagram to show that the 8 − N rule in the ELI-D/QTAIM representation is also applicable to prototype Zintl phases, semiconductors, and insulators. The deviations are also within $\bar{N}_{acc}^{ELI}(C^E) = 8 \pm 0.3$, except GaAs (+0.48), NaP (−0.63), and Na_2S_2 (−0.67); see the Supporting Information. In GaAs, the deviation originates from a larger mismatch between the Aufbau and the ELI-D shell populations. In the two Zintl phases NaP and Na_2S_2, the deviation is caused by a relative overpopulation of the lone-pair (lp) basins compared to the homopolar (cb) bonding basins, e.g., $\bar{N}(B_{lp}^S) = 2.13$ and $\bar{N}(B_{cb}^S) = 0.91$.[50]

Figure 8 shows the new conceptual correspondence between the compounds with homopolar/closed-shell and heteropolar

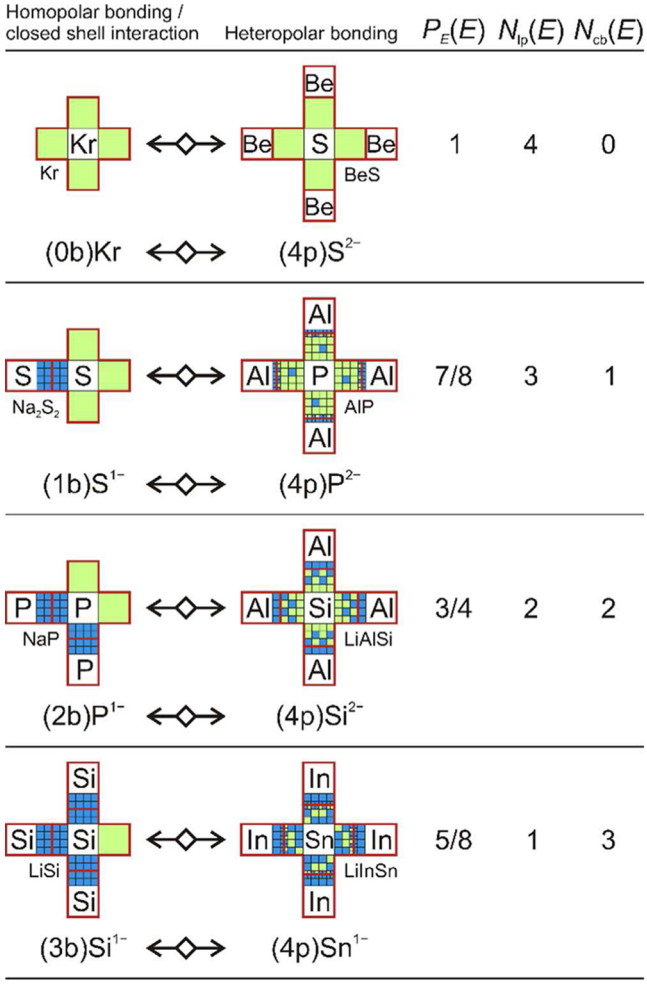

Figure 8. 8 − N rule from the ELI-D/QTAIM perspective: conceptual correspondence of bonding patterns in compounds with homopolar/closed-shell interactions (0b−3b, left) and with heteropolar bonding (4p, right). Only the valence region of the central atom is shown completely. The displayed $P_E(E)$, $N_{lp}(E)$, and $N_{cb}(E)$ are rounded for illustration. The special arrow symbol indicates the described correspondence between the compounds with (0b−3b)E and (4p)E bonding patterns.

DOI: 10.1021/acs.inorgchem.5b00135
Inorg. Chem. 2015, 54, 3970−3978

interactions in the framework of the 8 − N rule. The displayed $P_E(E)$, $N_{lp}(E)$, and $N_{cb}(E)$ are intentionally rounded to integers to ease the comparison. According to the 8 − N rule, an atom with 4, 5, 6, 7, or 8 valence electrons realizes the respective bonding patterns (4b), (3b, 1lp), (2b, 2lp), (1b, 3lp), and (4lp), where b stands for two-center-two-electron nonpolar bond and lp for a two-electron lone pair (see right panel of Figure 8).

The ELI-D/QTAIM intersection perspective yields the correspondence between the bonding pattern of the noble gas or compounds from the left panel and the bonding within the MgAgAs-type or zinc-blende-type phases on the right side. All atoms E in the MgAgAs-type compounds realize the bonding pattern (4p) with four equal heteropolar bonds, which are interpreted as a superposition of a partial nonpolar covalent part b′ and a polar hidden lone-pair part lp′

$$(4p) = (4x\mathrm{b}', 4[1 - x]\mathrm{lp}') \quad (15)$$

where x depends on the particular features of the contributing elements, e.g., electronegativity difference (x = 1 for the nonpolar bond and x = 0 for the fully polar interaction). The case of four lone pairs per atom occurs either for the noble gas atom (4lp) with van der Waals interaction to the environment or for sulfur in the ionic zinc-blende-type compound BeS (4p with very small x). Three lone pairs and one covalent bond occur for sulfur in the phase Na_2S_2 (1b, 3lp). An equivalent of three lone pairs (cf. hidden lone-pair character above) and one nonpolar bond are mixed in four heteropolar bonds in AlP (4p with x larger as in BeS). In the same way, the remaining compounds in Figure 8 illustrate the correspondence between homopolar/closed-shell interaction and heteropolar bonding for the cases with two and one lone-pair per anion.

CONCLUSIONS

The chemical bonding in main-group MgAgAs-type compounds A′AE within the present real-space approach displays a coexistence of ionic and covalent interactions. In the main-group representatives of the MgAgAs structure type, the continuous development from the mainly ionic to the network polyanionic bonding is quantified by several quantum chemical direct-space bonding indicators.

The direct-space representation and extension of the 8 − N rule allows the MgAgAs-type semiconductors to be classified as compounds with 8 − N covalent bonds. The heteropolar bonds in MgAgAs-type compounds are understood as a superposition of a nonpolar covalent part and a polar (hidden lone pair) part. The balance between covalent and lone-pair (nonpolar and polar) character is calculated quantum chemically with the ELI-D/QTAIM intersection technique. It changes depending on the particular anion that quantifies the polarity of the interaction. This way, MgAgAs-type compounds are interpreted in one line with zinc-blende-type, antifluorite-type, and Zintl phases with homopolar bonding and ionic closed-shell interactions. The traditional 8 − N rule formulation remains unchanged. However, within the present view, a component's number of covalent bonds is not necessarily equal to its coordination number. Thus, the 8 − N rule can be formulated for coordination numbers larger than four and other than (pseudo)tetrahedral coordination. On the other hand, the approach opens the possibility of characterizing the bonding in nonoctet compounds.

ASSOCIATED CONTENT

Supporting Information

Details of the topological analysis of ELI-D in MgAgAs-type and zinc-blende-type compounds as well as in the Zintl phases included in Figure 8. This material is available free of charge via the Internet at http://pubs.acs.org.

AUTHOR INFORMATION

Corresponding Author

*E-mail: grin@cpfs.mpg.de.

Notes

The authors declare no competing financial interest.

REFERENCES

(1) Graf, T.; Felser, C.; Parkin, S. S. P. *Prog. Solid State Chem.* **2011**, *39*, 1−50.
(2) Casper, F.; Graf, T.; Chadov, S.; Balke, B.; Felser, C. *Semicond. Sci. Technol.* **2012**, *27*, 063001.
(3) Repins, I.; Contreras, A.; Egaas, B.; DeHart, J.; Scharf, J.; Perkins, C. L.; To, B.; Noufi, R. *Prog. Photovoltaics* **2008**, *16*, 235−239.
(4) Kandpal, H. C.; Felser, C.; Seshadri, R. *J. Phys. D: Appl. Phys.* **2006**, *39*, 776−785.
(5) Kieven, D.; Klenk, R.; Naghavi, S.; Felser, C.; Gruhn, T. *Phys. Rev. B* **2010**, *81*, 075208.
(6) Tobola, J.; Pierre, J. *J. Alloys Compd.* **2000**, *296*, 243−252.
(7) Rowe, D. M. *Thermoelectrics Handbook: Macro to Nano*; CRC/Taylor and Francis: Boca Raton, FL, 2006.
(8) Canfield, P. C.; Thompson, J. D.; Beyermann, W. P.; Lacerda, A.; Hundley, M. F.; Peterson, E.; Fisk, Z.; Ott, H. R. *J. Appl. Phys.* **1991**, *70*, 5800−5802.
(9) Karla, I.; Pierre, J.; Skolozdra, R. V. *J. Alloys Compd.* **1998**, *265*, 42−48.
(10) Casper, F.; Felser, C. *Solid State Commun.* **2008**, *148*, 175−177.
(11) Fisk, Z.; Canfield, P. C.; Beyermann, W. P.; Thompson, J. D.; Hundley, M. F.; Ott, H. R.; Felder, E.; Maple, M. B.; Lopez de la Torre, M. A.; Visani, P.; Seaman, C. L. *Phys. Rev. Lett.* **1991**, *67*, 3310−3313.
(12) Goll, G.; Marz, M.; Hamann, A.; Tomanic, T.; Grube, K.; Yoshino, T.; Takabatake, T. *Phys. B* **2008**, *403*, 1065−1067.
(13) Müchler, L.; Casper, F.; Yan, B.; Chadov, S.; Felser, C. *Phys. Status Solidi RRL* **2013**, *7*, 91−100.
(14) Nowotny, H.; Sibert, W. *Z. Metallkd.* **1941**, *33*, 391−394.
(15) Juza, R.; Hund, F. *Z. Anorg. Chem.* **1948**, *257*, 1−12.
(16) Bende, D.; Grin, Yu.; Wagner, F. R. *Chem.—Eur. J.* **2014**, *20*, 9702−9708.
(17) Carlsson, A. E.; Zunger, A.; Wood, D. M. *Phys. Rev. B* **1985**, *32*, 1386−1389.
(18) Mellouki, A.; Bennecer, B.; Kalarasse, F. *J. Phys.: Condens. Matter* **2009**, *21*, 305402.
(19) Kandpal, H. C.; Felser, C.; Seshadri, R. *J. Phys. D: Appl. Phys.* **2006**, *39*, 776−785.
(20) Offernes, L.; Ravindran, P.; Kjekshus, A. *J. Alloys Compd.* **2007**, *439*, 37−54.
(21) Ackerbauer, S.-V.; Senyshyn, A.; Borrmann, H.; Burkhardt, U.; Ormeci, A.; Rosner, H.; Schnelle, W.; Gamza, M.; Gumeniuk, R.; Ramlau, R.; Bischoff, E.; Schuster, J. C.; Weitzer, F.; Leithe-Jasper, A.; Tjeng, L. H.; Grin, Yu. *Chem.—Eur. J.* **2012**, *18*, 6272−6283.
(22) Perdew, J. P.; Burke, K.; Ernzerhof, M. *Phys. Rev. Lett.* **1996**, *77*, 3865−3868.
(23) *Elk*, version 1.4.22; www.elk.sourceforge.net.
(24) Kohout, M. *DGrid*, version 4.7; Radebeul, Germany, 2013.
(25) Bader, R. F. W. *Atoms in Molecules*; Oxford University Press: Oxford, 1990.
(26) Ángyán, J. G.; Loos, M.; Mayer, I. *J. Phys. Chem.* **1994**, *98*, 5244−5248.
(27) Baranov, A. I.; Kohout, M. *J. Comput. Chem.* **2011**, *32*, 2064−2076.

DOI: 10.1021/acs.inorgchem.5b00135
Inorg. Chem. 2015, 54, 3970−3978

(28) Börrnert, C.; Grin, Y.; Wagner, F. R. *Z. Anorg. Allg. Chem.* **2013**, *639*, 2013−2024.
(29) Kohout, M. *Int. J. Quantum Chem.* **2004**, *97*, 651−658.
(30) Wagner, F. R.; Bezugly, V.; Kohout, M.; Grin, Y. *Chem.—Eur. J.* **2007**, *13*, 5724−5741.
(31) Wagner, F. R.; Kohout, M.; Grin, Y. *J. Phys. Chem. A* **2008**, *112*, 9814−9828.
(32) Becke, A. D.; Edgecombe, K. E. *J. Chem. Phys.* **1990**, *92*, 5397−5403.
(33) Kohout, M.; Savin, A. *Int. J. Quantum Chem.* **1996**, *60*, 875−882.
(34) Baranov, A. I. *J. Comput. Chem.* **2014**, *35*, 565−585.
(35) Kohout, M. *Faraday Discuss.* **2007**, *135*, 43−54.
(36) Raub, S.; Jansen, G. *Theor. Chem. Acc.* **2001**, *106*, 223−232.
(37) Fulton, R. L. *J. Phys. Chem.* **1993**, *97*, 7516−7529.
(38) Fulton, R. L. *J. Phys. Chem. A* **2006**, *110*, 12191−12203.
(39) Kuriyama, K.; Yamashita, Y.; Ishikawa, T.; Kushida, K. *Phys. Rev. B* **2007**, *75*, 233204.
(40) Kuriyama, K.; Kushida, K. *Solid State Commun.* **1999**, *112*, 429−432.
(41) Kuriyama, K.; Yamashita, Y.; Suzuki, Y.; Matsumoto, K.; Kushida, K. *AIP Conf. Proc.* **2010**, *1199*, 67−68.
(42) Nowotny, H.; Holub, F. *Monatsh. Chem.* **1960**, *91*, 877−887.
(43) Barth, J.; Fecher, G. H.; Schwind, M.; Baleanu, A.; Felser, C.; Shkabko, A.; Weidenkaff, A.; Hanss, J.; Reller, A.; Köhne, M. *J. Electron. Mater.* **2010**, *39*, 1856−1860.
(44) Bockelmann, W.; Schuster, H.-U. *Z. Anorg. Allg. Chem.* **1974**, *410*, 241−250.
(45) Becher, H. J. *Z. Anorg. Allg. Chem.* **1962**, *317*, 346−352.
(46) Silvi, B.; Savin, A. *Nature* **1994**, *371*, 683−686.
(47) Silvi, B.; Savin, A.; Wagner, F. R. In *Modelling of minerals and silicated materials*; Silvi, B., D'Arco, P., Eds.; Kluwer: Boston, MA, 1997; p 179.
(48) Grin, Y.; Savin, A.; Silvi, B. In *The Chemical Bond: Fundamental Aspects of Chemical Bonding*; Frenking, G., Shaik, S., Eds.; Wiley-VCH: Weinheim, Germany, 2014.
(49) Pauling, L. *The Nature of the Chemical Bond*; Cornell University Press: Ithaca, NY, 1960; p 431f.
(50) The typically found overpopulation (w.r.t. the conceptual value of two electrons) of the lone-pair ELI-D basins and the according underpopulation of the bond basins connected to the same atom needs further elaboration in the present ELI-D/QTAIM approach to the $8 - N$ rule. If these deviations are within an acceptable range, as is the case for the compounds studied above, then the approach provides interesting conceptual insights.

DOI: 10.1021/acs.inorgchem.5b00135
Inorg. Chem. 2015, 54, 3970−3978